

# Motion Parameter Selection for Flight Simulators

Karl D. Bilimoria<sup>1</sup> and Scott E. Reardon<sup>2</sup>  
*NASA Ames Research Center, Moffett Field, CA 94035*

**A motion flight simulator attempts to produce pilot-station accelerations that are similar to those experienced in the actual vehicle whose flight is being simulated. Due to travel limits of simulator hardware, the motion drive commands are based on a reduced form of the desired accelerations. A methodology is presented to select the best motion parameters (washout frequencies and attenuation gains) for flight simulation. This is accomplished by formulating a constrained optimization problem that provides the best possible matching of accelerations, coordinated across all motion axes, while satisfying motion state constraints arising from simulator hardware limits. The methodology is exercised using a Space Shuttle approach and landing trajectory. Results show that the surge and pitch accelerations produced by the optimized motion parameters provided a substantially (~45%) better match with the desired accelerations, compared to a standard set of motion gains that were manually developed over many years using heuristics and a trial-and-error process. In the other motion axes, the optimization parameters provided accelerations that were better than, or as good as, those provided by the standard parameters.**

## Introduction

Flight simulators are used for a variety of purposes including training, research/development, and accident investigation. Some flight simulators have a fixed base while others have a motion platform. Many simulation exercises attempt to provide a more realistic flight experience by presenting motion cues to the pilot. The vestibular system of the inner ear is an important motion sensor in the human body [1]: the semicircular canals can detect rotational accelerations as low as  $0.1 \text{ deg/s}^2$ , while the otoliths can detect non-gravity translational accelerations as low as  $0.07 \text{ ft/s}^2$ .

The goal of motion flight simulation is to produce accelerations of sufficient fidelity that pilots would fly the simulator in a way similar to how they would fly the actual aircraft. The simulator attempts to produce, within the constraints of its travel limits, pilot-station accelerations that are similar to the accelerations that would be experienced in the actual vehicle whose flight is being simulated. For a six-degree-of-freedom (6-DOF) motion simulator, this matching is performed for the three components of translational acceleration and the three components of rotational acceleration (or rotational velocity on some simulators). A perfect 1:1 motion match is generally not possible due to the motion travel limits of the simulator hardware. Hence the low-frequency components of pre-processed desired accelerations are washed out while the high-frequency components are attenuated, and these filtered acceleration signals are used to generate simulator cab motion drive commands. For a 6-DOF simulator, this motion tuning is accomplished by the appropriate selection of six attenuation gains and six washout frequencies, collectively referred to in this work as motion parameters. In practice, the motion parameters are generally determined by an *ad hoc* iterative process based on experience and heuristics, taking into account the desired acceleration profiles as well as simulator motion limits.

However, a comprehensive approach to motion tuning should account for the complex interactions between the motion axes. The rotational (roll/pitch/yaw) motion of the simulator cab induces false translational (surge/sway/heave) acceleration cues due to the moment arm between the cab's center-of-rotation and pilot station; some residual effects will remain even if the motion system logic attempts to compensate by modifying the translational drive commands. Additionally, most motion simulators have a residual tilt feature that rotates the cab to hold a steady roll/pitch angle so that the gravity vector provides a persistent sway/surge acceleration cue. Residual tilt provides the benefit of adding back some of the low-frequency translational acceleration content filtered by washout; however this introduces motion coupling between the roll-sway and pitch-surge axes resulting in false rotational acceleration cues. Another source of roll-sway motion coupling arises from the turn coordination feature found on

<sup>1</sup> Research Aerospace Engineer, Flight Trajectory Dynamics & Controls Branch, Mail Stop 210-10; [karl.bilimoria@nasa.gov](mailto:karl.bilimoria@nasa.gov). Associate Fellow, AIAA.

<sup>2</sup> VMS Lab Manager, Aerospace Simulation Research and Development Branch, Mail Stop 243-6; [scott.reardon@nasa.gov](mailto:scott.reardon@nasa.gov).

many motion simulators. Due to these factors, improving the motion fidelity along one axis may erode motion fidelity along other axes. The focus of this work is to develop an objective methodology that quickly and reliably generates an optimized set of motion parameters that provide the best possible motion fidelity coordinated across all axes of the trajectory being simulated while conforming with the motion travel limits of the flight simulator hardware.

This paper is organized as follows. The next section begins with an overview of existing guidelines for motion fidelity, and then presents a new coordinate transformation that may provide better intuition/insight for motion parameter tuning. The following section formulates the motion parameter selection process as a constrained optimization problem. Next, results are presented for a Space Shuttle final approach and landing trajectory, followed by conclusions.

## Motion Fidelity

Motion tuning is typically done by selecting appropriate values of attenuation gains ( $G$ ) and washout frequencies ( $\Omega$ ). The motion filter is a high-pass filter that washes out signal content at frequencies below  $\Omega$ , while scaling down high-frequency signal content according to the attenuation gain  $G$ . For a 1:1 motion match,  $G = 1$  and  $\Omega = 0$ . Since a perfect motion match is rarely possible, in general  $G < 1$  and  $\Omega > 0$ . As  $G$  becomes smaller and/or  $\Omega$  becomes larger, the simulator's motion fidelity deteriorates. Inside a region of ( $G$ ,  $\Omega$ ) space near the point  $G = 1$  and  $\Omega = 0$ , the accelerations produced by the flight simulator motion are of high fidelity, i.e., similar to actual flight. Within a medium-fidelity region adjacent to this high-fidelity region, the simulator-produced accelerations are noticeably different from actual flight but may still be acceptable. Outside the medium-fidelity region, the accelerations produced by the flight simulator are of low fidelity, i.e., sufficiently different from actual flight that they may be objectionable.

Guidelines for flight motion simulation fidelity were originally developed by Sinacori [2, 3], and later modified by Schroeder and Chung [4, 5]. The modified Sinacori guidelines from Ref. 5 are shown in Fig. 1. The ellipse segments in Fig. 1 can be described mathematically as:

$$\left(\frac{K-1}{a}\right)^2 + \left(\frac{P}{b}\right)^2 = 1 \quad (1)$$

where  $K$  is the magnitude ratio of the motion filter frequency response at 1 rad/s,  $P$  is the phase angle error (deg) of the motion filter frequency response at 1 rad/s, and the ellipse parameters  $a$  and  $b$  are given by:

	High/Medium Fidelity Boundary	Medium/Low Fidelity Boundary
<b>Translation</b>	$a = 0.4$ ; $b = 35$ deg	$a = 0.6$ ; $b = 60$ deg
<b>Rotation</b>	$a = 0.6$ ; $b = 35$ deg	$a = 0.8$ ; $b = 60$ deg

Since motion tuning is typically done using attenuation gains ( $G$ ) and washout frequencies ( $\Omega$ ), it is desirable to transform the motion fidelity boundaries from the ( $K$ ,  $P$ ) space of Fig. 1 to ( $G$ ,  $\Omega$ ) space. For a second-order motion filter often used by flight simulators, with  $\zeta (= 0.7)$  as the damping ratio, we have:

$$K = \frac{G}{\sqrt{(\Omega^2 - 1)^2 + (2\zeta\Omega)^2}} \quad (2)$$

$$P = \tan^{-1}\left(\frac{2\zeta\Omega}{1 - \Omega^2}\right) \quad (3)$$

For a given value of  $\Omega$ , the corresponding value of  $P$  is calculated from Eq. (3). Using this value of  $P$  in Eq. (1) provides the value of  $K$ . The value of  $G$  is then calculated from Eq. (2). Using the ( $G$ ,  $\Omega$ ) pairs from this process, a set of transformed motion fidelity boundaries can be constructed.

Figure 2 shows curves in ( $G$ ,  $\Omega$ ) space for medium and high fidelity boundaries, for a second-order motion filter, corresponding to Schroeder's modified-Sinacori boundaries of Fig. 1. The transformed curves in ( $G$ ,  $\Omega$ ) space may be more intuitive/insightful for motion parameter tuning than the "raw" modified-Sinacori curves in ( $K$ ,  $P$ ) space.

For example, it is immediately apparent, without computing frequency response properties of the motion filter, that high fidelity in the translational axes requires an attenuation gain greater than 0.6 and a washout frequency less than  $0.41 \text{ rad/s}^2$ .

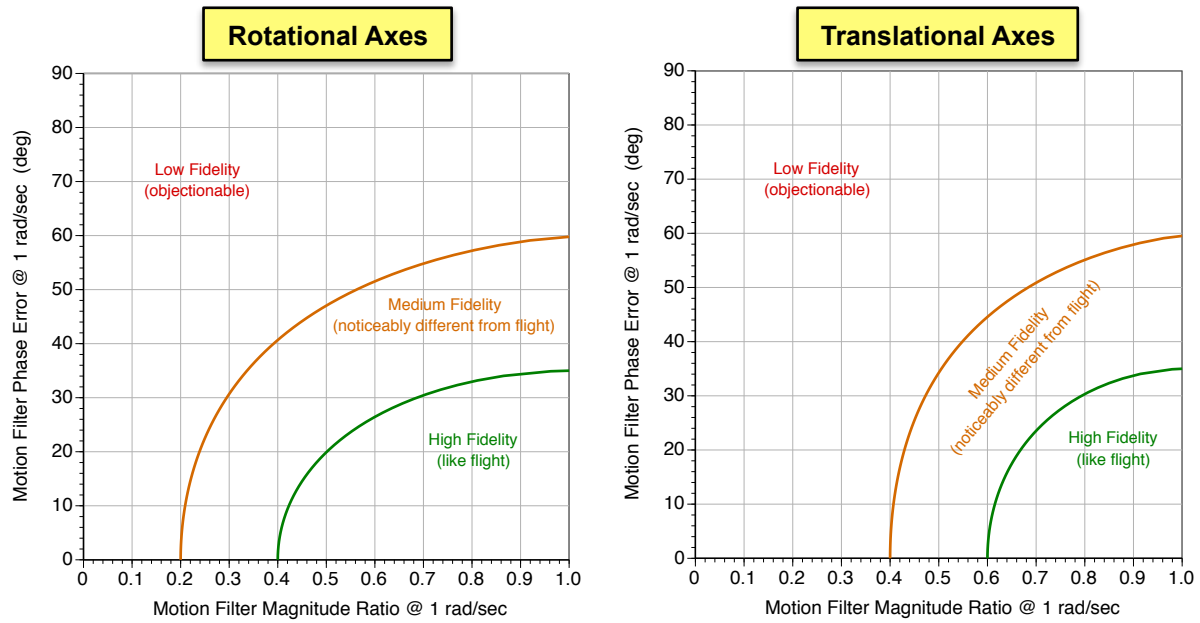


Fig. 1. Modified-Sinacori motion fidelity regions in  $(K, P)$  space – reproduced from Fig. 78 of Ref. 4

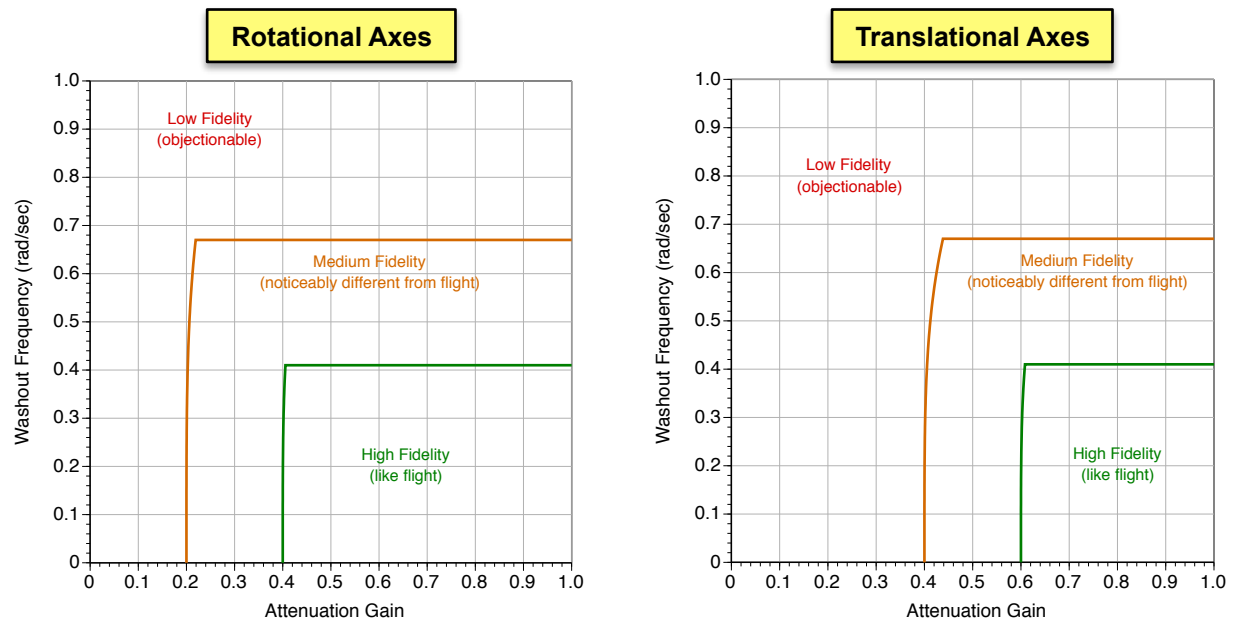


Fig. 2. Modified-Sinacori motion fidelity regions transformed to  $(G, Q)$  space for a 2<sup>nd</sup> order motion filter

### Illustrative Example

To illustrate some motion cueing features, the double-pulse signal shown in Fig. 3 (black) is used for the desired pilot-station translational accelerations  $A_{surge}^*$ ,  $A_{sway}^*$ , and  $A_{heave}^*$ ; the desired rotational accelerations,  $A_{roll}^*$ ,  $A_{pitch}^*$ , and  $A_{yaw}^*$  are all identically zero. The attenuation gains ( $G$ ) for all six axes were set to 0.75 and the washout frequencies ( $\Omega$ ) for all six axes were set to 0.3 rad/s, placing the entire motion parameter set inside the high-fidelity boundaries of Fig. 2. These input signals and motion parameters were run through the motion drive program of the NASA-Ames Vertical Motion Simulator (VMS) [6]. The output signals were the translational accelerations delivered at the pilot c.g. in the simulator cab,  $A_{surge}$ ,  $A_{sway}$ ,  $A_{heave}$ , and the simulator cab's rotational accelerations  $A_{roll}$ ,  $A_{pitch}$ , and  $A_{yaw}$ . In the perfect 1:1 motion case, the output signals would be identical to the input signals.

Results were computed for three separate conditions; each condition had zero rotational acceleration inputs, i.e., ( $A_{roll}^* = A_{pitch}^* = A_{yaw}^* = 0$ ). The translational acceleration inputs were as follows:

- Condition #1:  $A_{surge}^*$  was a double-pulse as shown in Fig. 3 (black);  $A_{sway}^* = 0$ ; ( $A_{heave}^* + g$ ) = 0
- Condition #2:  $A_{sway}^*$  was a double-pulse as shown in Fig. 3 (black);  $A_{surge}^* = 0$ ; ( $A_{heave}^* + g$ ) = 0
- Condition #3: ( $A_{heave}^* + g$ ) was a double-pulse as shown in Fig. 3 (black);  $A_{surge}^* = 0$ ;  $A_{sway}^* = 0$

The primary output for Condition #1 is  $A_{surge}$ , shown in Fig. 3 (blue). The effect of the 0.75 attenuation gain is clearly visible. It can also be seen that  $A_{surge}$  is washed out over the first few seconds as the residual tilt is washed in and reaches steady-state. Noting that  $A_{pitch}^* = 0$ , the false rotational cue due to the residual tilt wash-in can be seen in Fig. 4 in the time history of the simulator cab pitch acceleration  $A_{pitch}$  (blue).

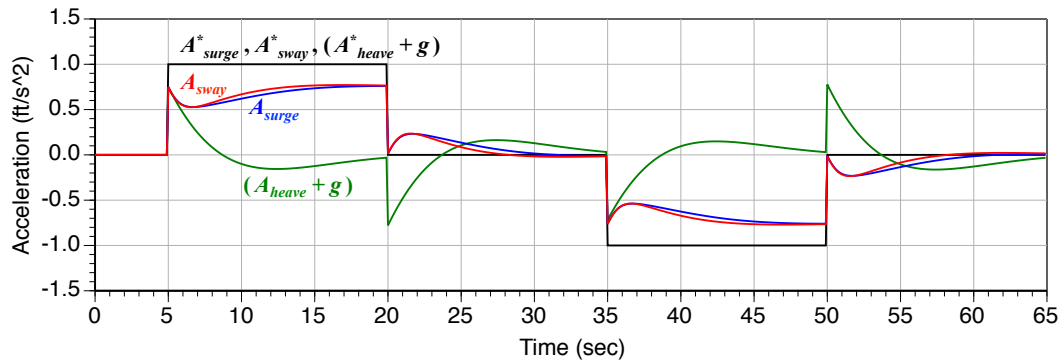


Fig. 3. Translational acceleration components vs. time

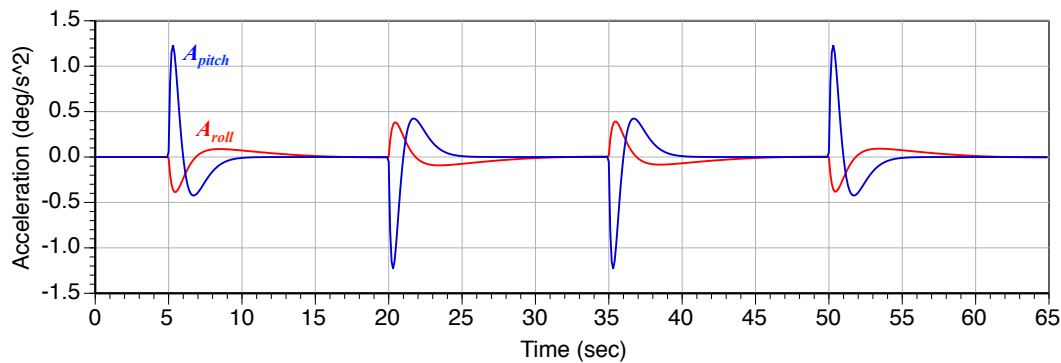


Fig. 4. Rotational acceleration components vs. time

The primary output for Condition #2 is  $A_{sway}$ , shown in Fig. 3 (red). Its behavior is qualitatively similar to that of  $A_{surge}$ . However, the time histories are not identical even though  $A_{sway}^*$  is identical to  $A_{surge}^*$ . This is because the horizontal translational axes of the VMS have very different travel lengths. Consequently, the VMS motion drive logic uses different equations for its initial processing of  $A_{surge}^*$  (short axis) and  $A_{sway}^*$  (long axis) inputs. Additionally, the VMS residual tilt dynamics are different for the long and short horizontal axes; this can be seen in Fig. 4 where the “spikes” of  $A_{roll}$  (red) are much smaller than those of  $A_{pitch}$  (blue).

The primary output of Condition #3 is  $(A_{heave} + g)$ , shown in Fig. 3 (green). Its behavior is qualitatively quite different from that of both  $A_{surge}$  and  $A_{sway}$ . The primary reason is that there is no residual tilt for the vertical axis.

### Optimization of Motion Parameters

This section presents a formal methodology to generate a set of motion parameters optimized for the trajectory being simulated (although some subsequent manual fine-tuning may be performed). The relationships between the simulator cab pilot-station translational accelerations ( $A_{surge}$ ,  $A_{sway}$ ,  $A_{heave}$ ) and the desired pilot-station translational accelerations ( $A_{surge}^*$ ,  $A_{sway}^*$ ,  $A_{heave}^*$ ) indicate the fidelity of translational motion cues. Similarly, the fidelity of rotational motion cues is indicated by the relationships between the simulator cab rotational accelerations ( $A_{roll}$ ,  $A_{pitch}$ ,  $A_{yaw}$ ) and the desired rotational accelerations ( $A_{roll}^*$ ,  $A_{pitch}^*$ ,  $A_{yaw}^*$ ). The fidelity (or equivalently the error) of motion cues is a function of the motion parameter set  $\bar{P}_{mot}$ , where:

$$\bar{P}_{mot} = \{ (G_{surge}, G_{sway}, G_{heave}, G_{roll}, G_{pitch}, G_{yaw}), (\Omega_{surge}, \Omega_{sway}, \Omega_{heave}, \Omega_{roll}, \Omega_{pitch}, \Omega_{yaw}) \} \quad (4)$$

In Eq. (4) above,  $G_{( )}$  and  $\Omega_{( )}$  correspond to the attenuation gain and washout frequency, respectively, along the corresponding axis. The motion parameter selection problem is to determine a set  $\bar{P}_{mot}^*$  that minimizes the errors between the desired and achieved acceleration components while satisfying the motion travel constraints  $\bar{M}_{travel} \leq \bar{M}_{travel}^{max}$ , where  $\bar{M}_{travel}$  represents the simulator motion states (position, velocity, etc.) in all axes and  $\bar{M}_{travel}^{max}$  represents the motion state limits (possibly coupled in some states) of the simulator hardware.

Given a time history of desired pilot-station accelerations ( $A_{surge}^*$ ,  $A_{sway}^*$ ,  $A_{heave}^*$ ,  $A_{roll}^*$ ,  $A_{pitch}^*$ ,  $A_{yaw}^*$ ) over a time interval of interest  $[0, T]$  and a candidate set of motion parameters  $\bar{P}_{mot}$ , one can calculate corresponding time histories for simulator cab pilot-station accelerations ( $A_{surge}$ ,  $A_{sway}$ ,  $A_{heave}$ ,  $A_{roll}$ ,  $A_{pitch}$ ,  $A_{yaw}$ ) using the motion drive program. A motion-cue error metric is defined as:

$$E_{MC} = w_{surge} \frac{\int_0^T (A_{surge}(t) - A_{surge}^*(t))^2 dt}{\int_0^T (A_{surge}^*(t))^2 dt} + w_{sway} \frac{\int_0^T (A_{sway}(t) - A_{sway}^*(t))^2 dt}{\int_0^T (A_{sway}^*(t))^2 dt} + w_{heave} \frac{\int_0^T (A_{heave}(t) - A_{heave}^*(t))^2 dt}{\int_0^T (A_{heave}^*(t))^2 dt} \\ + w_{roll} \frac{\int_0^T (A_{roll}(t) - A_{roll}^*(t))^2 dt}{\int_0^T (A_{roll}^*(t))^2 dt} + w_{pitch} \frac{\int_0^T (A_{pitch}(t) - A_{pitch}^*(t))^2 dt}{\int_0^T (A_{pitch}^*(t))^2 dt} + w_{yaw} \frac{\int_0^T (A_{yaw}(t) - A_{yaw}^*(t))^2 dt}{\int_0^T (A_{yaw}^*(t))^2 dt} \quad (5)$$

where  $w_{( )}$  are weighting factors associated with the error in each channel.

Noting that  $E_{MC}$  is an implicit function of  $\bar{P}_{mot}$ , and that perfect simulation fidelity corresponds to a zero value of  $E_{MC}$ , the determination of the best motion parameter set  $\bar{P}_{mot}^*$  can be posed as a state-constrained parameter optimization problem:

$$\bar{P}_{mot}^* = \min_{\bar{P}_{mot}} \{E_{MC}(\bar{P}_{mot})\}, \text{ subject to the motion state constraints } \bar{M}_{travel} \leq \bar{M}_{travel}^{\max} \quad (6)$$

## Results

The motion parameter optimization problem was applied to a VMS simulation of a Space Shuttle trajectory for final approach, landing, and rollout. At simulation start, the Shuttle is at an altitude of 10,000 ft and a groundspeed of 329 kts, at a distance of 5.8 nmi from the runway threshold. A pre-flare maneuver is initiated at an altitude of 1,900 ft, which occurs 42 sec into the simulation. Main-gear touchdown occurs at 75 sec, followed by nose-gear touchdown at 90 sec; the simulation is terminated a few seconds later. State histories along the trajectory were generated and recorded, with an auto-land system providing control inputs to the Shuttle flight dynamics model. Figure 5 shows the time histories of key state variables.

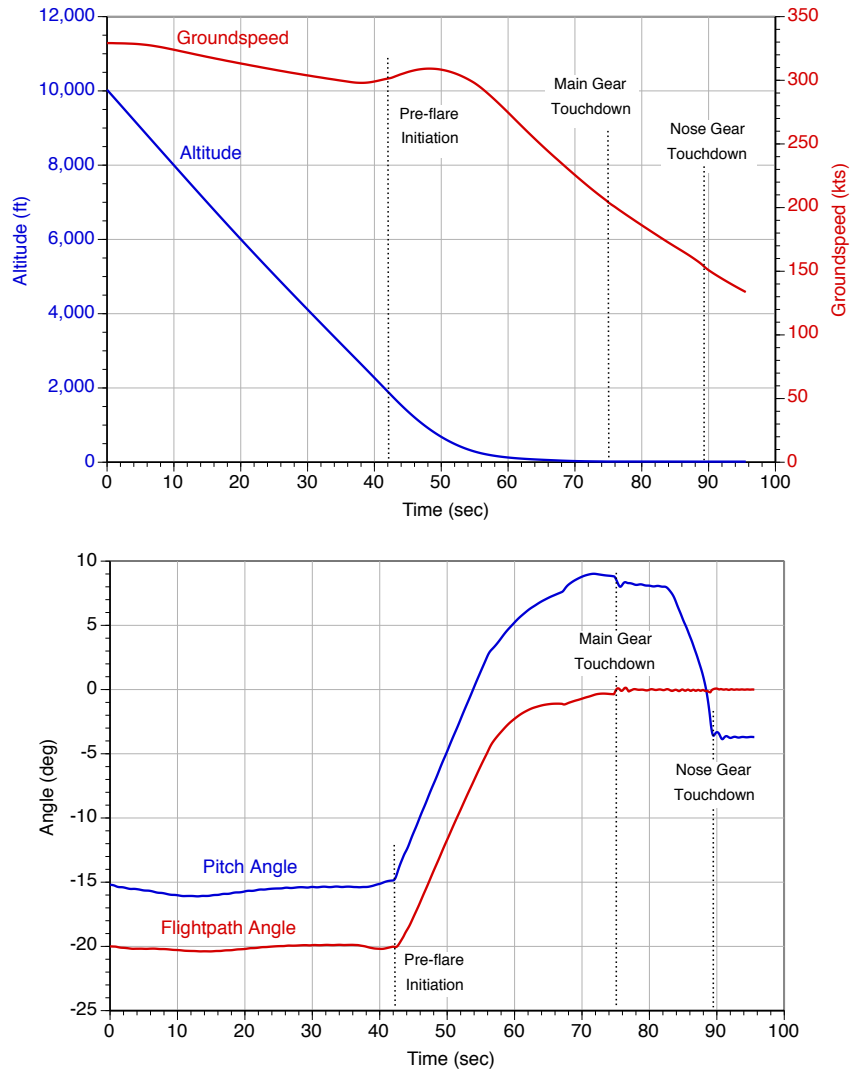


**Fig. 5. Time histories of key state variables for Space Shuttle approach and landing**

The desired pilot-station translational accelerations,  $A_{surge}^*$ ,  $A_{sway}^*$ ,  $(A_{heave}^* + g)$ , and the desired rotational accelerations,  $A_{roll}^*$ ,  $A_{pitch}^*$ , and  $A_{yaw}^*$  were computed along the trajectory. These accelerations are shown in Fig. 6.

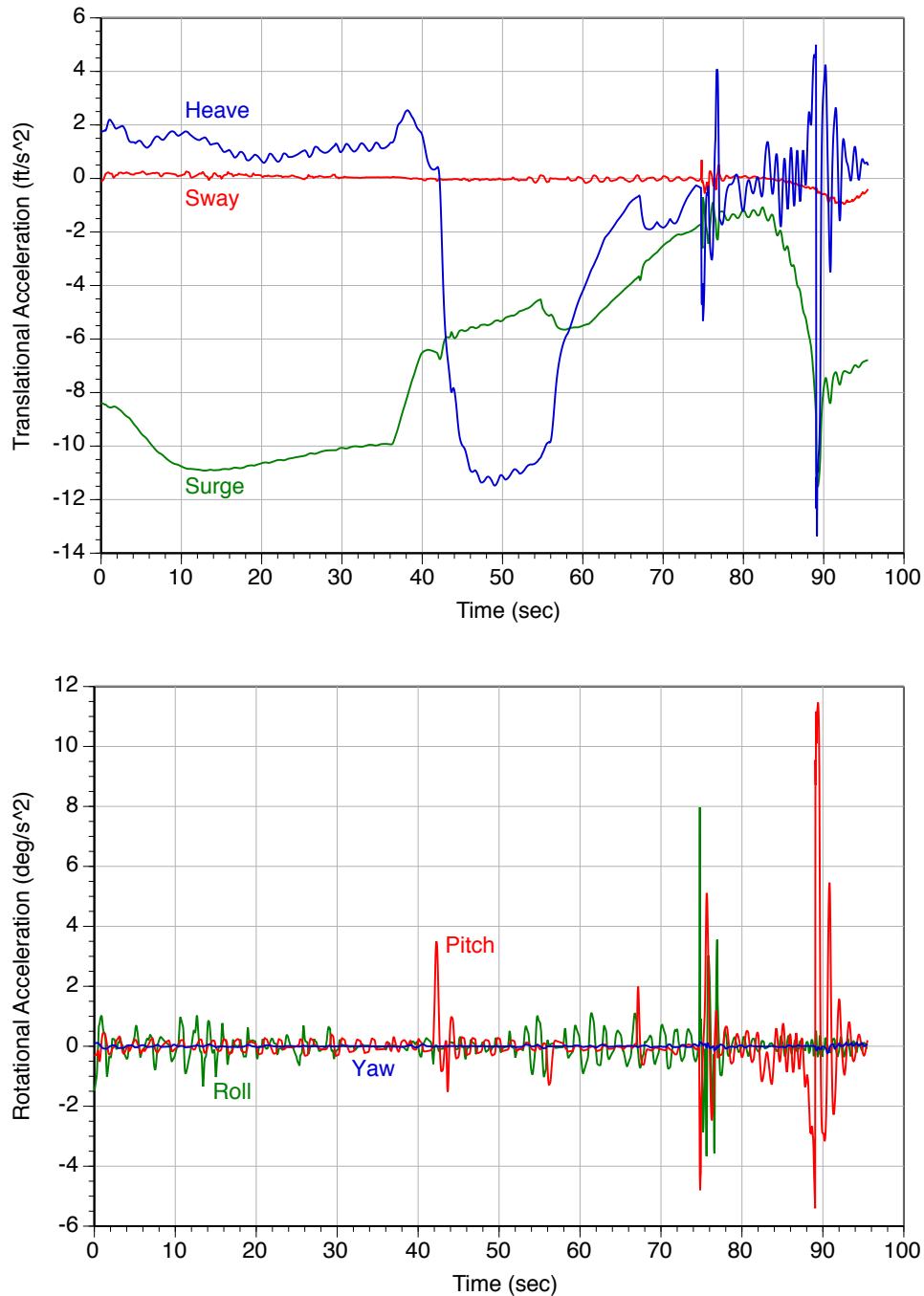


**Fig. 6. Time histories of desired pilot-station accelerations**

It can be seen that the desired surge and heave accelerations are quite large, with sustained values in excess of  $0.35g$ . The desired sway accelerations are very small because the trajectory involves minimal lateral dynamics, although there are some spikes around main-gear and nose-gear touchdown times. In the rotational axes, the desired

pitch accelerations exhibit substantial spikes around pre-flare initiation, main-gear touchdown, de-rotation, and nose-gear touchdown. The desired roll accelerations exhibit substantial spikes around main-gear touchdown, and also feature oscillations with an amplitude on the order of 1 deg/s<sup>2</sup> over most of the trajectory due to turbulence effects. The desired yaw accelerations are essentially negligible, mostly remaining inside the threshold of human motion perception.

Based on the above observations, it was determined that the emphasis on motion fidelity should be high in the surge and heave axes, moderate in the pitch axis, and low in the sway, roll, and yaw axes. Accordingly, the weights in the optimization performance index of Eq. (6) were set to:  $w_{surge} = 10$ ,  $w_{sway} = 1$ ,  $w_{heave} = 10$ ,  $w_{roll} = 1$ ,  $w_{pitch} = 5$ ,  $w_{yaw} = 1$ .

A MATLAB function, *fmincon*, was used to solve the constrained optimization problem posed in Eq. (6). It solves a nonlinear multivariable optimization problem, leveraging the “interior point” algorithm to find the constrained minimum of a nonlinear scalar function of multiple variables starting from an initial estimate [7]. The exit criteria for the first-order optimality measure and the relative change in input arguments were set to  $10^{-3}$  and  $10^{-2}$ , respectively.

During normal operations of the VMS, motion state limits are enforced by a software routine called ALARMS: Adjustable Limiting Algorithms for Robust Motion Simulation [8]. These algorithms utilize limiting functions based on simulator cab position, velocity, acceleration, and jerk along all six motion axes. The limiting functions involve combinations of states; for example, an impending velocity limit violation is handled more aggressively if the corresponding acceleration is higher. During the motion parameter optimization process, enforcement of position limits (surge =  $\pm 3$  ft, sway =  $\pm 15$  ft, heave =  $\pm 22$  ft, roll =  $\pm 14$  deg, pitch =  $\pm 14$  deg, yaw =  $\pm 19.5$  deg) was intentionally disabled in ALARMS to enable the MATLAB optimizer *fmincon* to enforce these position limits as a state inequality constraint. Velocity, acceleration, and jerk limits were enforced by ALARMS, external to the MATLAB optimizer.

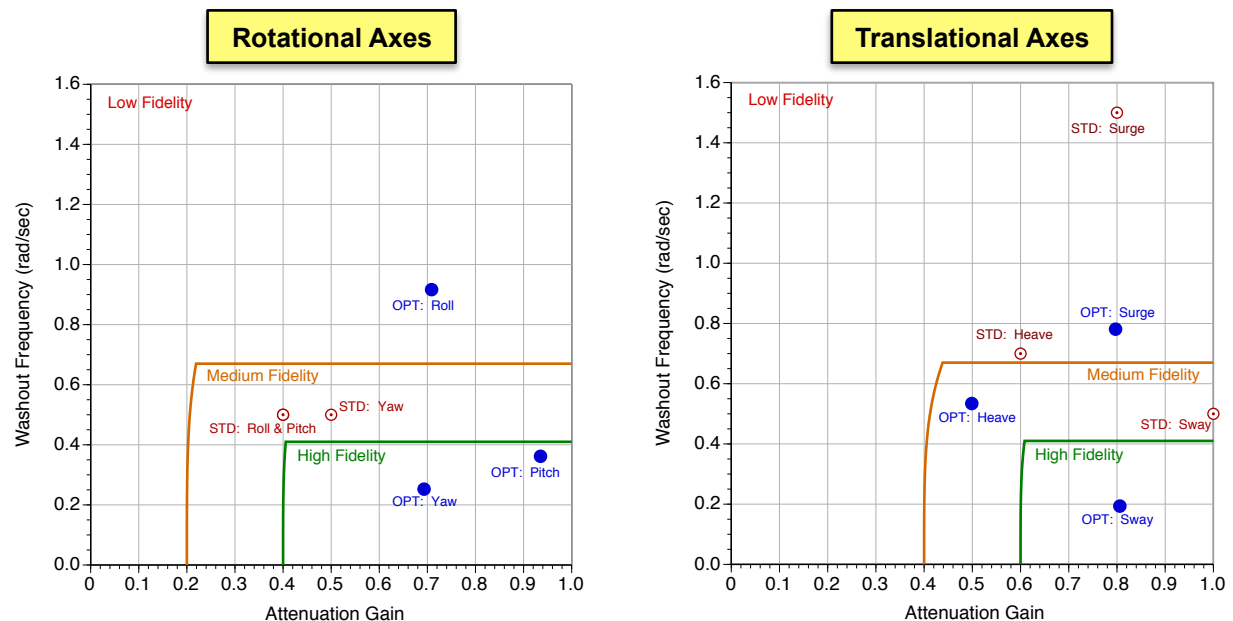


**Fig. 7. Standard and optimized motion parameters relative to motion fidelity regions**

Optimized motion parameters from the converged solution were compared with the “standard” motion parameters traditionally used for VMS simulations of Shuttle approach and landing. This set of standard motion parameters was developed manually by VMS simulation engineers over many years of Shuttle approach/landing simulation experience, using heuristics and a trial-and-error process in consultation with Shuttle pilots. Figure 7 shows both sets of motion parameters against the backdrop of the motion fidelity regions that were presented in Fig. 2. It can be seen that for all three translational axes, the optimized parameters lie in a better motion fidelity



region of  $(G, \Omega)$  space than the standard parameters. In the rotational axes, the optimized parameters for pitch and yaw also lie in a better motion fidelity region of  $(G, \Omega)$  space than the standard parameters. For the roll axis, the attenuation gain is better (larger), but the washout frequency is worse (larger), placing the optimized parameters in the low fidelity region rather than the medium fidelity region where the standard roll parameters are placed. However, as will be shown later in this section, the optimized parameters still provide a better match with the desired roll acceleration time history. This is partly due to the relatively low accelerations required in the roll axis, and partly due to the motion fidelity boundaries being general/soft guidelines rather than absolute truths. Moreover, the simulator cab displacement in the roll axis was quite small ( $\sim 10\%$  of travel limit), and hence the roll motion parameters could likely be manually adjusted into the medium fidelity region without violating motion travel limits. Alternatively, the optimization process could be run again after assigning a higher weight for the roll acceleration error in the performance index. This discussion highlights the point that while the optimized motion parameters provide a good solution for direct use, there may also be opportunities for *post hoc* enhancements by experienced simulation engineers who are able to incorporate factors not explicitly included in the mathematical formulation of the original optimization problem.

In this work, the primary metric for motion fidelity is the error between the desired pilot-station accelerations and the actual accelerations experienced in the simulator cab in response to simulator motion drive commands generated using a set of motion parameters. Figure 8 compares the desired surge acceleration profile with the accelerations produced using standard and optimized motion parameters. Figures 9 to 11 show corresponding data for the heave, roll, and pitch axes, respectively. In each case, it can be seen that the accelerations produced using optimized parameters provide a better match with the desired accelerations at most points in time.

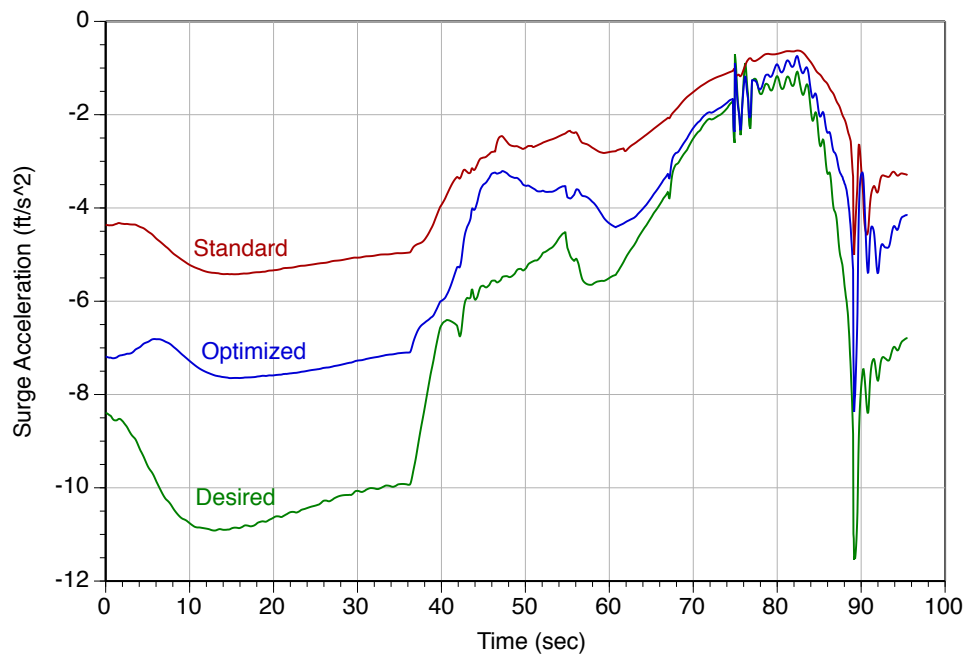


**Fig. 8. Desired surge accelerations and those produced by standard and optimized parameters**

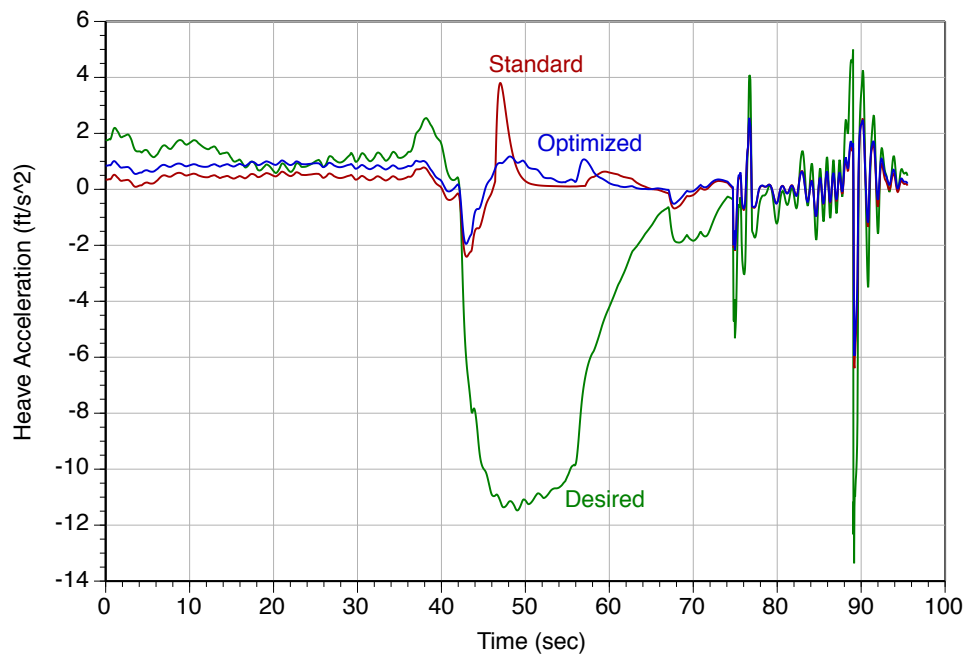


**Fig. 9. Desired heave accelerations and those produced by standard and optimized parameters**

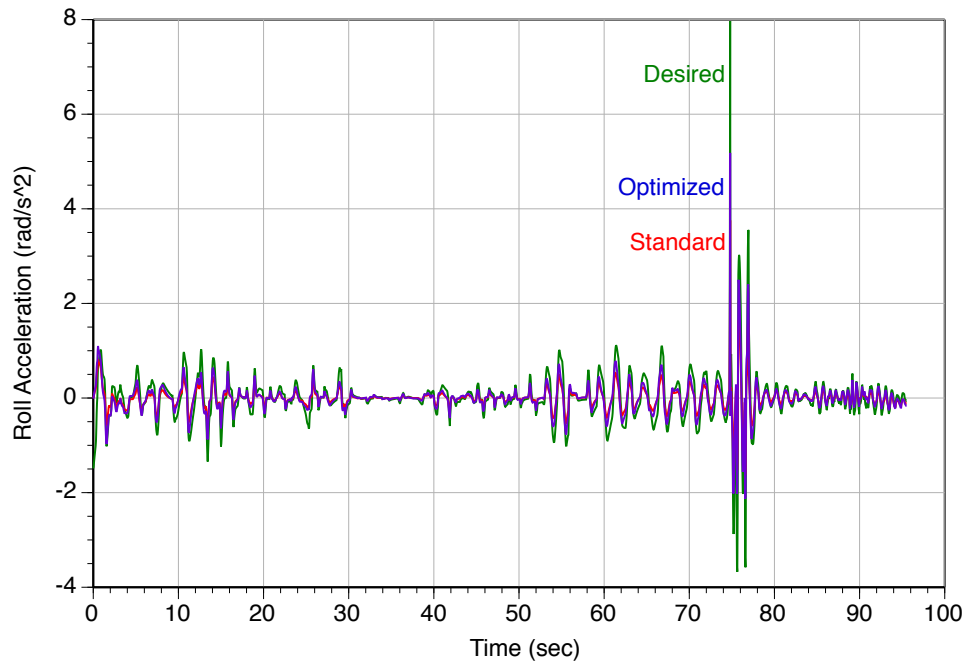


**Fig. 10. Desired roll accelerations and those produced by standard and optimized parameters**

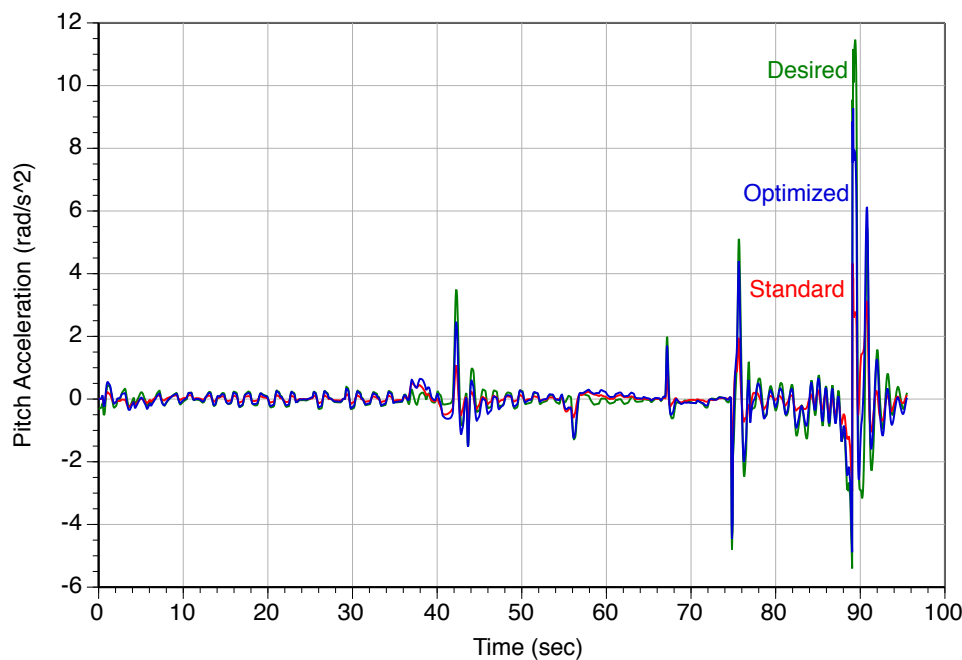


**Fig. 11. Desired pitch accelerations and those produced by standard and optimized parameters**

To provide an aggregated metric of motion fidelity, the root mean square (RMS) error over the acceleration time history was computed for each motion axis. Figure 12 shows RMS errors (between desired and actual values) of translational and rotational accelerations for the two cases: one using standard motion parameters, and the other using optimized motion parameters.

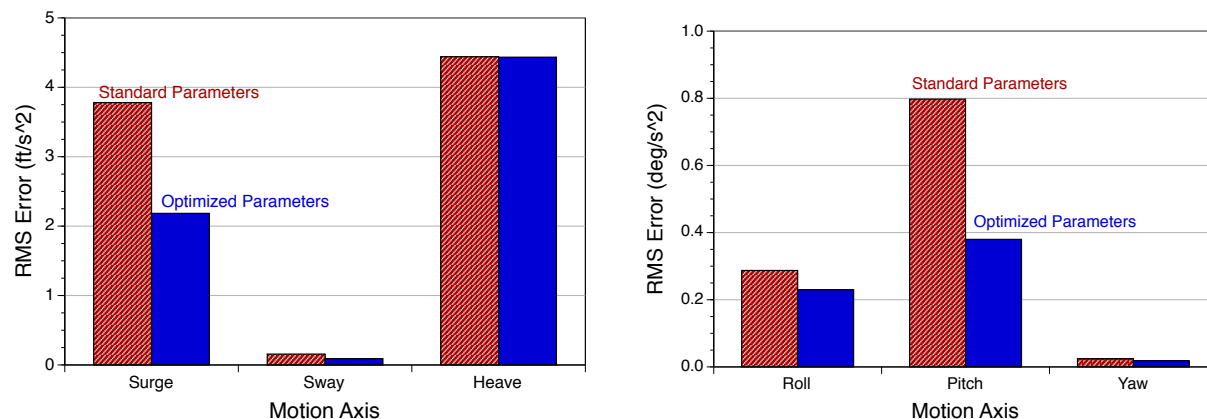


**Fig. 12. RMS errors between desired and actual acceleration time histories**

It can be seen that for the surge and pitch axes there is a 42% and 52% reduction, respectively, in RMS errors for optimized parameters compared to RMS errors for standard parameters. There is a 20% reduction in RMS error for the roll axis. The RMS errors in the sway and yaw axes are very small for both standard parameters and optimized parameters (which do provide a small reduction in error) because the corresponding desired accelerations are very small due to the dynamics of the trajectory (see Fig. 6). There is a negligibly small reduction in the aggregate RMS error for the heave axis, but it can be seen from Fig. 9 that the heave accelerations produced using optimized parameters provide a slightly better match with the desired heave accelerations at most points in time.

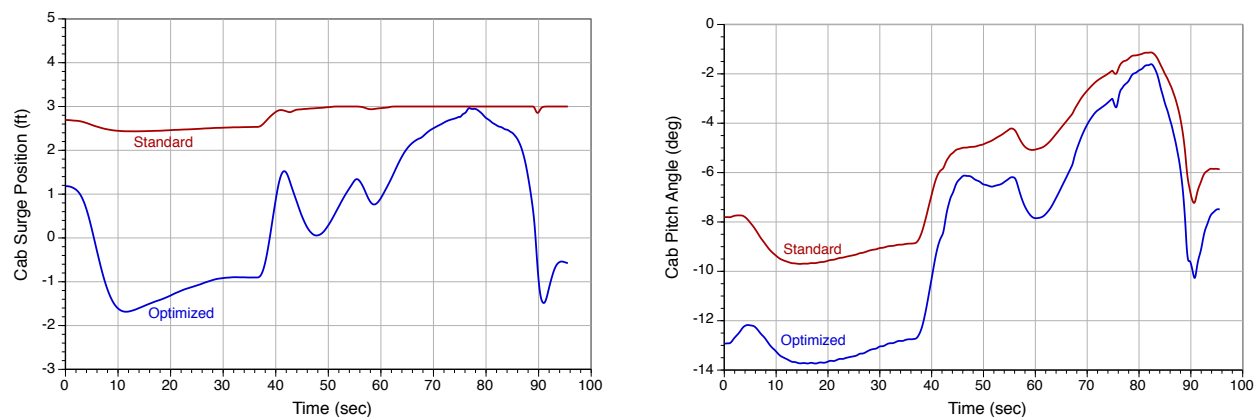


**Fig. 13. Motion travel for standard and optimized parameters: surge axis (left) and pitch axis (right)**

The improvements in motion fidelity (acceleration matching) correspond to an increase in the motion travel utilization along the appropriate axes. Figure 13 shows simulator cab travel, for standard and optimized motion parameters, along the surge and pitch axes. In both those axes, the cab displacements for optimized parameters are just inside the simulator travel limits (enforced during the optimization process). For actual simulator use the motion parameters would be selected to utilize ~85% of available motion travel for an “average” trajectory flown by human pilots, to provide a simulator travel margin that accommodates a range of variations in piloting techniques. Due to this reduction in allowed simulator travel, the improvement in motion fidelity would be correspondingly less than that reported above. On the other hand, there are additional motion-related simulator parameters that could be included in the optimization process to enhance motion fidelity. These parameters include simulator cab initial (simulation run start) states, as well as parameters associated with the simulator dynamics of residual tilt and turn coordination.

## Conclusions

A methodology has been presented for quickly and reliably selecting motion parameters for flight simulation. One contribution of this work is the coordinate transformation of existing motion fidelity region boundaries to a domain that is more intuitive for motion parameter tuning. The main contribution of this work is the formulation of a constrained optimization problem that provides the best possible matching of accelerations, coordinated across all motion axes, while satisfying motion state constraints arising from simulator hardware limits.

The methodology is exercised using a Space Shuttle approach and landing trajectory, utilizing all of the available motion travel on the VMS. Results show that the surge and pitch accelerations produced by the optimized motion parameters provide a substantially (~45%) better match with the desired accelerations, compared to a standard set of motion gains that was manually developed over many years using heuristics and a trial-and-error process. For the roll axis, there is a 20% improvement in acceleration matching. In the other three motion axes, the optimization parameters provide accelerations that are slightly better than, or as good as, those provided by the standard parameters.

## Acknowledgment

The authors thank Dr. Jeffery Schroeder of the Federal Aviation Administration for useful technical discussions over the course of this work.

## References

1. Rolfe, J.M. and Staples, K.J., *Flight Simulation*, Cambridge Aerospace Series, 1986, pp. 112.
2. Sinacori, J.B., “A Practical Approach to Motion Simulation,” Paper No. 73-931, *AIAA Visual and Motion Simulation Conference*, Palo Alto, CA, 1973.
3. Sinacori, J.B., “The Determination of Some Requirements for a Helicopter Flight Research Simulation Facility,” NASA CR-152066, 1977.
4. Schroeder, J.A., and Chung, W.W.Y., “Simulation Motion Requirements for Coordinated Maneuvers,” *Journal of the American Helicopter Society*, Vol. 46, No. 3, 2001, pp. 175-181.

5. Schroeder, J.A., "Helicopter Flight Simulation Motion Platform Requirements," NASA/TP-1999-208766, July 1999, pp. 60.
6. Aponso, B.L., Beard, S.D., and Schroeder, J.A., "The NASA Ames Vertical Motion Simulator – A Facility Engineered for Realism," Royal Aeronautical Society Flight Simulation Conference, London, U.K., June 2009.
7. MATLAB function *fmincon*, <http://www.mathworks.com/help/optim/ug/fmincon.html> [cited 20 May 2015].
8. McFarland, R.E., "Adjustable Limiting Algorithms for Robust Motion Simulation," Paper No. 2001-4305, *AIAA Modeling and Simulation Technologies Conference*, Montreal, Canada, August 2001.